Bilayer manganites reveal polarons in the midst of a metallic breakdown

F. Massee[1†], S. de Jong[1†], Y. Huang[1], W. K. Siu[1], I. Santoso[1], A. Mans[1], A. T. Boothroyd[2], D. Prabhakaran[2], R. Follath[3], A. Varykhalov[3], L. Patthey[4], M. Shi[4], J. B. Goedkoop[1] and M. S. Golden[1]★

The origin of colossal magnetoresistance (CMR) in manganese oxides is among the most challenging problems in condensed-matter physics today. The true nature of the low-temperature electronic phase of these materials is heavily debated. By combining photoemission and tunnelling data, we show that in the archetypal bilayer system $La_{2-2x}Sr_{1+2x}Mn_2O_7$, polaronic degrees of freedom win out across the CMR region of the phase diagram. This means that the generic ground state of bilayer manganites supports a vanishing coherent quasi-particle spectral weight at the Fermi level throughout k-space. The incoherence of the charge carriers, resulting from strong electron–lattice interactions and the accompanying orbital physics, offers a unifying explanation for the anomalous charge-carrier dynamics seen in transport, optics and electron spectroscopies. The stacking number N is the key factor for true metallic behaviour, as an intergrowth-driven breakdown of the polaronic domination to give a metal possessing a traditional Fermi surface is seen in this system.

Competition between local lattice distortions leading to anti-ferromagnetic, charge and orbital (CO) ordering on the one hand, and mixed valence character promoting metallic ferromagnetic double exchange on the other, determines the transport properties[1] of the manganite materials family and is proposed to lie at the root of their colossal magnetoresistance (CMR) effect[2]. $(La,Sr)_{N+1}Mn_NO_{3N+1}$, abbreviated LSMO (where N is the number of stacked MnO_2 planes between [La,Sr]O block layers[3]) exhibits a remarkable decrease in metallic character with decreasing N (ref. 4), see Supplementary Fig. S1. Metallic behaviour thrives in the phase diagram of cubic LSMO (ref. 5), whereas the bilayer analogue is metallic only in a narrow Sr-doping and temperature regime[6], giving rise to the largest CMR effect[7]. The more strongly 2D, single-layer compound shows neither metallic nor CMR behaviour[8].

Focusing on bilayer LSMO within the CMR region of the phase diagram, the prevailing picture from structural studies is one of polarons existing above T_C. On cooling towards T_C, these short-range versions of the CO order, typical of the insulating compositions, become increasingly correlated[9,10]. Eventually double exchange, leading to an itinerant, metallic state, takes over.

This metallic state for $x = 0.4$ has been shown to support small quasi-particles (QPs) in the spectral function as measured by angle-resolved photoemission (ARPES; ref. 11). These signal coherent electronic excitations, albeit strongly dressed with lattice distortions, are seen as evidence for a novel and elusive state of matter known as a polaronic metal[11,12].

Other ARPES studies paint a different picture, with stronger QP features observed at low T that persist up to temperatures of order $1.5T_C$ (refs 13–15), despite the system being nominally insulating. In contrast, scanning tunnelling microscopy/spectroscopy (STM/S) studies reported (pseudo)gaps in the local density of states near E_F for $x = 0.30$ (ref. 16) and 0.325 (ref. 17), both in the metallic and insulating temperature regimes. Finally, new neutron diffraction data for $x = 0.4$ has shown that even far below T_C—at 10 K in

the metallic state—polarons remain as fluctuations that strongly broaden and soften phonons close to the wave vectors where the charge order peaks would appear in the insulating phase[18].

Here, a combination of ARPES and STM/S reveals that the bilayer manganites still have a number of surprises in store. First, we show that the intrinsic spectral response of these systems is pseudogapped, with negligible coherent spectral weight at E_F anywhere in k-space at any temperature, across the CMR region of the phase diagram. Second, we show that the strong QP features seen in ARPES studies—also above T_C—are due to the unavoidable presence of $N > 2$ stacking-fault intergrowths.

These new insights clear the way for a unified interpretation of the physical properties of CMR bilayer LSMO in terms of strongly incoherent charge carriers, and suggest that local control of the dimensionality of such manganites—by means of tuning the stacking number, N—may offer a novel route to new functional nanostructures.

Imaging the cleavage surface of a typical bilayer LSMO single crystal in the CMR-doping region using low-temperature STM/S yields large, flat terraces, see Fig. 1a,b. One surprising characteristic of these STM data is that the surface atoms have proved extremely difficult to image. In the literature, the only reported observations of atomic resolution in bilayer LSMO concerned small nanometre-sized patches[16,17], and recently the difficulty of obtaining atomic resolution has been attributed to oxygen-defect dynamics[19]. The terraced, flat and debris-free surfaces we image may lack atomic corrugation, however they do possess a spatial texture in the tunnelling signal. These structures are usually disordered, but are—in some cases—ordered into a semi-regular, square-like lattice, exhibiting characteristic length scales of the order 2–3 nm, as can be seen in Fig. 1c. The quasi-ordered nature of these regions at the surface is evident from the autocorrelation traces of the STM topographs, as shown in Fig. 1d, which exhibit clear structures at distances ranging from 5 to 15 unit cells.

[1]Van der Waals-Zeeman Institute, University of Amsterdam, 1018XE Amsterdam, The Netherlands, [2]Clarendon Laboratory, Oxford University, OX1 3PU Oxford, UK, [3]BESSY GmbH, Albert-Einstein-Strasse 15, 12489 Berlin, Germany, [4]Paul Scherrer Institute, Swiss Light Source, CH-5232 Villigen, Switzerland. [†]These authors contributed equally to this work. *e-mail: M.S.Golden@uva.nl.
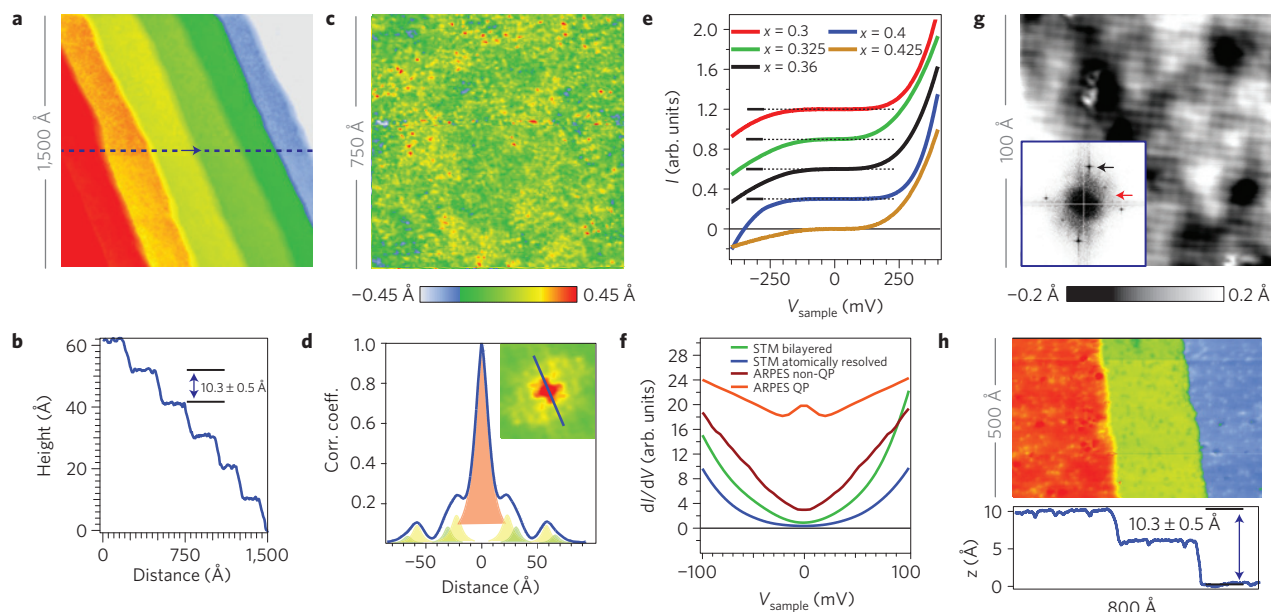
Figure 1 | STM/S on bilayer manganites ($T = 4.2$ K). a, Large field of view of a region with (an above average number of) half unit cell steps at the surface and **b** corresponding line scan ($x = 0.3$, $V = -500$ meV, $I = 20$ pA). **c**, Semi-ordered square-like texture for $x = 0.36$, ($V = -450$ meV, $I = 150$ pA), clearly seen in the line trace (**d**) through the centre of the autocorrelation (inset of **d**, 220×220 Å^2). A Lorentzian fit gives a correlation length of $\sim$2.3 nm. **e**, STS spectra showing a pseudogap > 100 meV ($V = 500$ meV, $I \approx 50$ pA) for all Sr-doping concentrations studied ($V = 500$ meV, $I \approx 50$ pA). The spectra are offset for clarity. **f**, Comparison between symmetrized, k-integrated ARPES spectra and STM dI/dV traces. **g**, Topograph showing atomic resolution ($V = 500$ meV, $I = 140$ pA) with (1×1) and $\sqrt{2} \times \sqrt{2}$ spots in the Fourier transform (inset, black and red arrows respectively), which are not found in the corresponding LEED images. **h**, Topography of the same region as **g**, where the step height corresponds to that expected for single layer LSMO.

Comparison with low-energy electron diffraction (LEED) data recorded in the STM chamber shows that the orientation of the quasi-periodic structures is not pinned to the underlying atomic lattice. The tunnelling spectra of bilayer LSMO from all cleavage surfaces measured are pseudogapped (symmetrically) around E_F over an energy range of several 100 meV at low temperature for all doping concentrations studied, as shown in Fig. 1e (in this context Supplementary Fig. S8 illustrates the insensitivity of the spectral form to the junction resistance in the different STS studies). The tunnelling spectra themselves show no major variations from point to point. This suggests that the observed spatial textures seen in the STM data are a subtle, 'higher order' structural ordering phenomenon, leading to modest, periodic signatures, slightly reminiscent of the 2.5 nm correlated regions seen in the high-T, polaronic liquid phase described in ref. 10. The authors of ref. 2 suggest that aggregates of polarons resembling a charge-ordered state should be observable in STM experiments above T_C. Our new data show that these kind of entities could exist at the surface even at low temperatures, possibly being a log-jammed form of the fluctuating polarons observed in recent neutron experiments[18].

During our STM investigation of numerous cleavage surfaces of bilayer LSMO, very clear atomic resolution was found over a large terrace of one particular cleave, shown in Fig. 1g. Analysis of the Fourier transform shows reduced in-plane symmetry, with clear $\sqrt{2} \times \sqrt{2}$ spots, shown in the inset to Fig. 1g. This is atypical for bilayer LSMO, which has a (1×1) tetragonal lattice symmetry in the ferromagnetic 'metallic' phase that we observe in all our LEED data (see Supplementary Fig. S2c). An important observation linked to this large-scale STM imaging with atomic contrast is that the step bordering this terrace is only one quarter of the $N = 2$ c axis unit cell in height (5 Å, see Fig. 1h). Furthermore, the near-E_F spectral weight in the STS spectra from this region is more strongly suppressed compared with those from non-atomically resolved regions exhibiting 10 Å step heights, as shown in Fig. 1f. Taken together, these facts form a compelling

argument that in Fig. 1g,h we are—in fact—imaging a stacking fault in the Ruddlesden–Popper manganite, in which an extra La$_2$O$_2$ block (or blocks) creates a region of the bilayer crystal which is effectively single layer (La,Sr)$_2$MnO$_4$. The fact that atomic contrast is readily observed in STM of $N = 1$ LSMO (ref. 20) further strengthens our interpretation.

The observation with STM/S of such a surface inclusion with a different stacking number N is rare, but is not, in itself, wholly surprising. Numerous muon spin rotation μSR studies[21], magnetization measurements[22,23] and transmission electron microscopy studies[24,25] have established that stacking faults occur even in the very best crystals at the $\approx 1\%$ level[22,23]. These intergrowths vary—locally—the stacking number N and are the cause of anomalous steps in the magnetization above the bulk T_C common in bilayer LSMO between 200 and 350 K: small patches with N values above two deliver a higher T_C. Owing to the strong connection between magnetism and metallic behaviour in the manganites, it is a simple step to reason that $N > 2$ intergrowths would also be metallic above and beyond the bilayer T_C. In contrast, an $N = 1$ intergrowth will be more insulating than bilayer LSMO, in keeping with the STM/S data shown in Fig. 1f.

Armed with a heightened awareness that (unavoidable) intergrowths in bilayer LSMO are present in real samples, and that signals from these regions can be picked up in spectroscopic experiments, we now turn to our ARPES investigations. In total, we have measured dozens of bilayer LSMO single crystals from two different sources, with Sr-doping levels spanning the entire CMR region of the phase diagram. ARPES spectra were taken at low temperature over a square grid across the samples in steps of 100 μm, see Fig. 2b. Using such a procedure, two types of spectral signature are observed on different locations: (1) from only 1–5% of the cleavage surface, sharp QP peaks are observed at all k-locations on the Fermi surface, as shown in Fig. 2c, and (2) a vanishingly small spectral weight is observed near E_F from the majority of the sample surface, as can be seen in Fig. 2a for 10 K and in
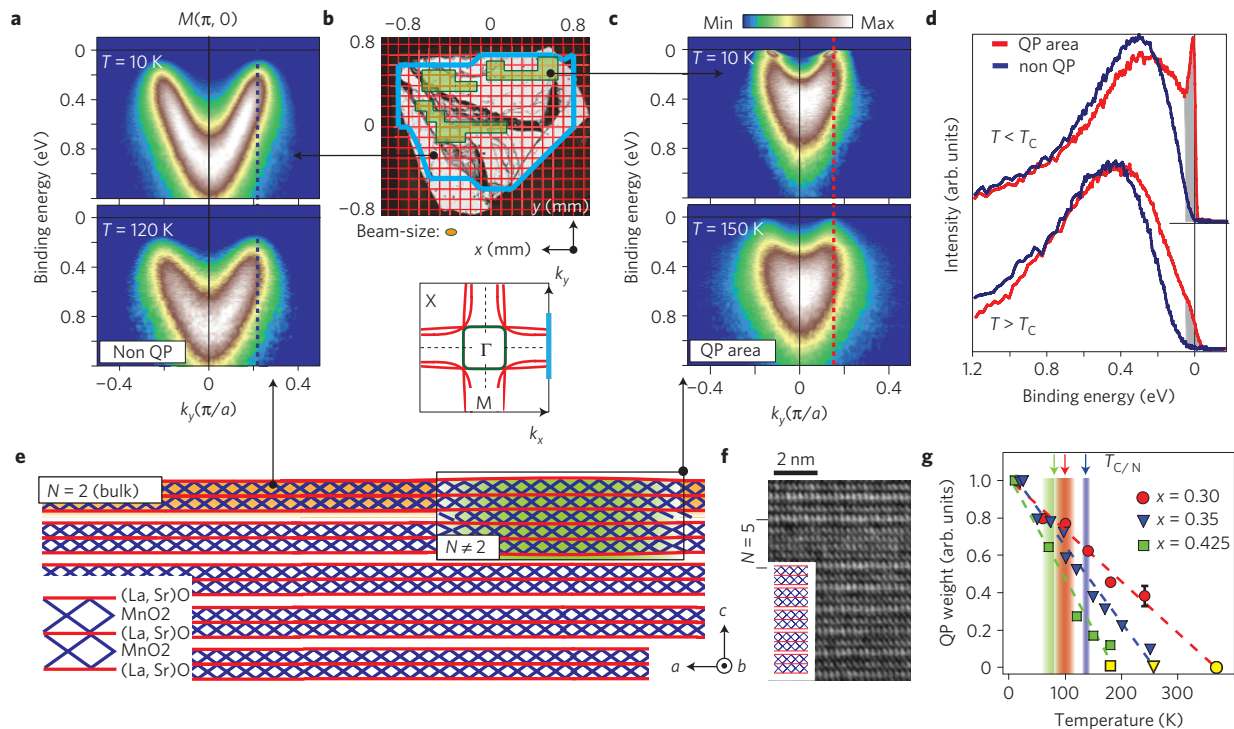
Figure 2 | Spatial ARPES mapping of bilayer LSMO. a, Typical $I(E,k)$-images at $(\pi,0)$ (k-space cut being shown in the schematic Brillouin zone below **b**, after ref. 48) for $T \ll T_C$ and $T \gg T_C$ from a non-QP-peaked region of the cleave ($x = 0.425$, $h\nu = 56$ eV). A clear absence of QP features characterizes the data both above and below the bulk T_C. **b**, Optical micrograph of the post-cleavage surface ($x = 0.36$). A spectrum was taken at each red grid point and the synchrotron radiation spot size is shown to scale. The (for this sample unusually abundant) regions which support QP peaks are green shaded. **c**, Analogous to **a** for a QP-peaked region of the same sample. **d**, $I(E)$-curves along the dashed lines in **a** and **c**. For the QP-peaked region, there remains significant spectral weight at E_F for 150 K, despite that $T \gg T_C$. **e**, Schematic side-on view of a cleaved bilayer LSMO crystal with a stacking fault (here an $N = 5$ intergrowth) at the crystal surface which supports QP states up to $T \gg T_C$. The intrinsic spectral signature is that seen in **a** and the blue traces in **d**. **f**, A transmission electron microscopy image, from ref. 23, showing an actual $N = 5$ inclusion. **g**, Relative QP spectral weight (integrated over $E_F \pm 75$ meV, grey shaded in **d**) versus T. The error bar indicates the uncertainty in the normalization of spectra at different T.

the comparison made in Fig. 2d. Figure 2 also shows the ARPES signatures from the non-QP-peaked and QP-peaked regions for $T > T_C$. For the non-QP-peaked regions, a modest shift in spectral weight to higher binding energies can be seen. For the minority, QP-peaked locations, the near-E_F spectral weight is reduced at 150 K (a temperature that is almost twice the bilayer T_C for this doping), however the $I(E)$ traces in Fig. 2d still exhibit considerable intensity at E_F, and certainly no signs of a pseudogap. Figure 2g shows that this anomalous behaviour—with quasi-particle peaks visible above T_C—occurs for doping levels spanning the whole CMR region, despite the fact that the vast majority of the sample volume in each case is in the paramagnetic, insulating regime. Further apparently anomalous behaviour is presented in Supplementary Figs S3 and S4, in which we show that for varying doping levels the Fermi surface (FS) topology (that is the number of bands) and the FS area from QP-peaked regions also deviate from what is expected for bilayer LSMO. Moreover, when observed for a particular doping, the QP peaks exhibit a cleave-to-cleave variation in the number of FS sheets observed around the X-point ranging from one to four.

Thus, combining our atomic scale tunnelling data with these ARPES data, it is clear that the strongly QP-peaked spectral signature is not representative of bilayer LSMO. Instead, the intrinsic signature of this material is that of a pseudogapped, very bad metal that supports vanishingly small QP spectral weight at E_F at any k-location. This may sound surprising for a metal, but the bilayer manganites are far from being normal metals. In the 'metallic' phase, the ab-plane resistivity is in excess of the Mott maximum of $10^{-3}\,\Omega$ cm (refs 26,27), which is very different unlike the situation in their cubic cousins (see Supplementary Fig. S1). In addition, the

optical conductivity of bilayer LSMO shows an incoherent Drude peak, even down to the lowest temperatures[28,29], again, unlike the situation in the $N = \infty$, cubic materials[30]. Therefore, it is clear that the strongly QP-peaked regions of the cleaves are simply signals from stacking faults[23] located sufficiently close to the crystal termination (Fig. 2e,f), which consequently contribute strongly to the near-E_F photoemission signal. In this manner, the anomalous temperature dependence of the QP peaks (Supplementary Fig. S4c) also falls naturally into place. Supplementary Fig. S5 provides additional arguments involving the orthorhombic crystal symmetry of the stacking fault regions observed in ARPES data; here we note that the inset to Fig. 1g already shows the orthorhombic surface of an intergrowth (in this case $N = 1$).

The new experimental data from real space and k-space probes presented above provide a unifying framework in which to understand all the published ARPES data, which is a welcome simplification. However, the bilayer manganites still present a richness—in particular in the form of a highly sensitive doping dependence—which is a major challenge to our theoretical understanding. We have examined our crystals using ARPES employing different polarization conditions and measurement geometries. Although in our experiments we have adopted a wide range of experimental conditions, including geometries and polarizations very similar to those of refs 11 and 12, we have not observed the nodal quasiparticles reported for the $x = 0.4$ composition. In contrast, Supplementary Fig. S6 shows that the strong QP features from the $N > 2$ intergrowths are robust with respect to a wide variation of the polarization and geometry conditions. The use of a high degree of in-plane polarization (as

related in ref. 11) did not uncover small QP-peaked structures close to E_F for any of the $x = 0.4$ cleaves or for the non-QP-peaked regions of any other doping levels. This may seem puzzling until one realizes that the phase diagram of bilayer LSMO possesses numerous line phases. Various narrow regions in the phase diagram show special types of magnetic and/or orbital ordering: $x = 0.30$ (AFM metal), 0.50 (CE-type charge and orbital ordering) and 0.60 (AFM metal)[31–33]. Remarkably, deviations of only 0.01 in doping level (for example away from $x = 0.60$; refs 33,34) have a major effect on the electronic behaviour. Accordingly, we suggest that exactly at, or very close to a composition of $x = 0.40$ there is also such a line phase, the exact composition of which has not been 'hit' in the ARPES data of refs 13–15,35,36.

Our data—covering samples right across the CMR region of the phase diagram—shows that the generic electronic signature of bilayer LSMO is that of a pseudogapped, very bad metal with vanishingly small QP spectral weight at the Fermi level. Hence, 'nodal metallicity', although of great interest in the context of comparisons with the high T_c superconducting cuprates, is apparently not a necessary factor for bringing about CMR behaviour, and seems to be confined to the doping level $x = 0.40$.

Before reaching a final conclusion as regards the physics behind a metal which has QP spectral weight below our detection limit, one further issue needs to be dealt with, that being whether the surface of bilayer LSMO is even less like a regular metal than the bulk. X-ray resonant diffraction has shown the first pair of MnO_2-planes nearest to the surface of bilayer LSMO cleaved in air[37,38] or in vacuum[39] to possess no ferromagnetic order, and thus the surface could be expected to exhibit non-metallic behaviour. A recent (hard) X-ray photoemission study of the same crystals as studied here found no major difference between the surface and bulk in terms of charge transfer or composition[40], thus the differences between the outermost bilayer and the rest are subtle in nature. Although recent LEED studies[39] have given no evidence for a lowering of the 2D surface symmetry, for example through a surface reconstruction, a finding our own LEED data support, a contraction of the apical bond length for the outermost MnO_2-plane was observed[39], which could impact the mobility of the charge carriers at the surface.

Here it is essential to realize that the photocurrent measured in ARPES certainly originates from deeper in the crystal than the first bilayer only, even at excitation energies in the vacuum ultraviolet. Therefore, we can conclude that the bad-metallic, fully pseudogapped behaviour we observe is indeed a genuine characteristic of the bulk for the vast majority of the CMR-compositions in bilayer LSMO. Although disentangling the spectral signatures of the outermost and deeper lying bilayers is difficult, we do note that the energy range at E_F over which the spectral weight is suppressed in ARPES is smaller than the negative bias gap seen in STM/S; the latter probing strictly the electronic states at the surface. This is evident from Fig. 1f, where STS spectra from bilayer LSMO and from the $N = 1$ intergrowth are compared with symmetrized, k-integrated photoemission spectra from ARPES maps (such as those in Supplementary Fig. S3) for a QP-peaked and a non-QP-peaked region of the surface.

We now return to the key issue of the physical nature of the charge carriers responsible for electronic transport of the bilayer manganites. The most suitable picture—considering the results on both the dynamics of the charge carriers and the subtle yet clear structural anomalies they bring with them—is that of polaronic charge carriers above T_C, but also in the ferromagnetic (bad) metallic state. The fact that the STM signatures of the weakly self-organized polaronic carriers, when 'log-jammed' at the surface, resemble the polaronic correlations seen above T_C suggests that in the bulk of the bilayer LSMO system—which is more metallic than the surface—the system teeters on the edge of a breakdown of the fragile polaronic metal state into an insulating, charge and orbitally

ordered state. This borderline situation, coupled to the disorder and enhanced fluctuations present in these quasi-2D systems, delivers all the ingredients for the colossal magnetoresistance transition[2].

We conclude this paper by making a connection back to the relationship between the materials physics and crystal chemistry of the manganite family. The physics describing the manganites depends crucially on the propensity of the system to form ordered textures in spin, charge and orbital occupation. For the polaronic metal state to remain stable, it is vital that the degeneracy in the e_g orbital manifold is preserved, as this is a necessary condition for the double-exchange energy reduction that encourages hopping of the carriers. This condition, in turn, stipulates equality in the equatorial and axial bond lengths of the MnO_6 octahedra. The deviating axial bond lengths at the surface of bilayered LSMO compared with the bulk, as observed in ref. 39, lift this degeneracy and thus push the surface of this material further into the insulating regime than the bulk: the correlated polarons can become static, as we observe with our STM measurements. On the other hand, the $N > 2$ inclusions we observe structurally bear greater resemblance to the cubic compound, and thus show a higher propensity towards metallic behaviour, including the existence of coherent spectral weight. Paradoxically, the fragility of the polaronic metal state in the bilayer systems is also the key to their colossal magnetoresistance, as it delivers the precarious balance between weakly metallic and insulating behaviour required for such an enormous sensitivity to the extra impulse provided by an external magnetic field.

The results presented here formulate a clear challenge to developing a general theory for the transport in $N = 2$ systems involving practically incoherent charge carriers—fluctuating polarons—while also capturing the sensitivity to the stacking number, N. Aside from the lattice polaron generally considered, different types of polaron, such as spin and orbital polarons, should be taken into consideration[41–43]. An interesting proposal for the charge carrier dynamics in the manganites is the existence of so-called Zener polarons[44,45]. In such a polaron, the charge carrier is not localized on a single manganese atom, but on two neighbouring manganese atoms which are ferromagnetically coupled by the Zener double-exchange mechanism. It has been shown that all these different types of polaron lead to a large incoherent spectral weight, such as is seen in our ARPES investigations[41–43,46].

The new insight we have gained points towards the great potential of, for example, layer-by-layer thin-film engineering to generate tailor-made heterostructures, not only to lead to enhanced transition temperatures[47], but in combination with modern lithographic and patterning methods to tune and improve magnetoresistive properties on the sub-micrometre scale in a new generation of complex oxide devices.

Methods

STM The STM data were recorded using a commercially variable temperature UHV microscope from Createc GmbH. Tungsten tips were prepared by electrochemical etching, followed by *in situ* conditioning before each measurement using a Au(788) single crystal. In all cases, the spectral shapes obtained were independent of the tip to sample distance, a sign of good vacuum tunnelling conditions. All investigated samples have been cleaved *in situ* before measuring. The crystallographic orientation was determined directly after the STM measurements, using *in situ* LEED. The set-up voltages, as well as the tunnelling currents, are indicated in the figures.

ARPES The angle-resolved photoemission data presented here were obtained using the following beamlines and end-stations: (1) the UE112-PGMa beamline at the Helmholtz Zentrum Berlin (BESSY II storage ring), Berlin, Germany, coupled to an SES100 analyser; (2) the UE112-PGMb beamline at BESSY, coupled to the R4000 analyser of the 1cubed end-station and (3) the SIS beamline at the Swiss Light Source (SLS), Villigen, Switzerland, equipped with an SES2002 analyser. The total experimental energy broadening at 20 K was set to 30 meV, 20 meV and 15 meV, for the three end-stations, respectively. The momentum resolution was $0.02\pi/a$ along the analyser slit at the excitation energies used. The photon energies used are indicated in the relevant figures. High-quality single crystals of

LSMO were grown both in Oxford and Amsterdam using optical floating zone techniques, and were cleaved *in situ* and characterized using LEED before ARPES measurements were conducted. For further details concerning the sample quality and characterization, see Supplementary Fig. S2.

References

1. Jin, S. *et al.* Thousandfold change in resistivity in magnetoresistive La–Ca–Mn–O films. *Science* **264,** 413–415 (1994).
2. Şen, C., Alvarez, G. & Dagotto, E. Competing ferromagnetic and charge-ordered states in models for manganites: The origin of the colossal magnetoresistance effect. *Phys. Rev. Lett.* **98,** 127202 (2007).
3. Goodenough, J. B. Theory of the role of covalence in the perovskite-type manganites [La, M(II)]MnO_3. *Phys. Rev.* **100,** 564–573 (1955).
4. Kimura, T. & Tokura, Y. Layered magnetic manganites. *Annu. Rev. Mater. Sci.* **30,** 451–474 (2000).
5. Urushibara, A. *et al.* Insulator–metal transition and giant magnetoresistance in $La_{1-x}Sr_xMnO_3$. *Phys. Rev. B* **51,** 14103–14109 (1995).
6. Moritomo, Y., Asamitsu, A., Kuwahara, H. & Tokura, Y. Giant magnetoresistance of manganese oxides with a layered perovskite structure. *Nature* **380,** 141–144 (1996).
7. Perring, T. G., Aeppli, G., Moritomo, Y. & Tokura, Y. Antiferromagnetic short range order in a two-dimensional manganite exhibiting giant magnetoresistance. *Phys. Rev. Lett.* **16,** 3197–3200 (1997).
8. Moritomo, Y., Tomioka, Y., Asamitsu, A., Tokura, Y. & Matsui, Y. Magnetic and electronic properties in hole-doped manganese oxides with layered structures: $La_{1-x}Sr_{1+x}MnO_4$. *Phys. Rev. B* **51,** 3297–3300 (1995).
9. Vasiliu-Doloc, L. *et al.* Charge melting and polaron collapse in $La_{1.2}Sr_{1.8}Mn_2O_7$. *Phys. Rev. Lett.* **83,** 4393–4396 (1999).
10. Campbell, B. J. *et al.* Structure of nanoscale polaron correlations in $La_{1.2}Sr_{1.8}Mn_2O_7$. *Phys. Rev. B* **65,** 014427 (2001).
11. Mannella, N. *et al.* Nodal quasiparticle in pseudogapped colossal magnetoresistive manganites. *Nature* **438,** 474–478 (2005).
12. Mannella, N. *et al.* Temperature-dependent evolution of the electronic and local atomic structure in the cubic colossal magnetoresistive manganite $La_{1-x}Sr_xMnO_3$. *Phys. Rev. B* **76,** 233102 (2007).
13. Sun, Z. *et al.* Quasiparticlelike peaks, kinks, and electron–phonon coupling at the $(\pi,0)$ regions in the CMR oxide $La_{2-2x}Sr_{1+2x}Mn_2O_7$. *Phys. Rev. Lett.* **97,** 056401 (2006).
14. Sun, Z. *et al.* A local metallic state in globally insulating $La_{1.24}Sr_{1.76}Mn_2O_7$ well above the metal–insulator transition. *Nature Phys.* **3,** 248–252 (2007).
15. de Jong, S. *et al.* Quasiparticles and anomalous temperature dependence of the low-lying states in the colossal magnetoresistant oxide $La_{2-2x}Sr_{1+2x}Mn_2O_7$ ($x = 0.36$) from angle-resolved photoemission. *Phys. Rev. B* **76,** 235117 (2007).
16. Rønnow, H. M., Renner, Ch., Aeppli, G., Kimura, T. & Tokura, Y. Polarons and confinement of electronic motion to two dimensions in a layered manganite. *Nature* **440,** 1025–1028 (2006).
17. de Santis, S. *et al.* Imaging of polarons in ferromagnetic bilayered manganites by scanning tunnelling microscopy. *J. Supercond. Nov. Magn.* **20,** 531–533 (2007).
18. Weber, F. *et al.* Signature of checkerboard fluctuations in the phonon spectra of a possible polaronic metal $La_{1.2}Sr_{1.8}Mn_2O_7$. *Nature Mater.* **8,** 798–802 (2009).
19. Bryant, B., Renner, Ch., Tokunaga, Y., Tokura, Y. & Aeppli, G. Imaging oxygen defects and their motion at a manganite surface. *Nature Commun.* **2,** 212 (2011).
20. Evtushinsky, D. V. *et al.* Bridging charge-orbital ordering and Fermi surface instabilities in half-doped single-layered manganite $La_{0.5}Sr_{1.5}MnO_4$. *Phys. Rev. Lett.* **105,** 147201 (2010).
21. Allodi, G. *et al.* Magnetic order in the double-layer manganites $(La_{1-x}Pr_z)_{1.2}Sr_{1.8}Mn_2O_7$: Intrinsic properties and role of intergrowth. *Phys. Rev. B* **78,** 064420 (2008).
22. Potter, C. D. *et al.* Two-dimensional intrinsic and extrinsic ferromagnetic behavior of layered $La_{1.2}Sr_{1.8}Mn_2O_7$ single crystals. *Phys. Rev. B* **57,** 72–75 (1998).
23. Bader, S. D., Osgood, R. M., Miller, D. J., Mitchell, J. F. & Jiang, J. S. Role of intergrowths in the properties of naturally layered manganite single crystals (invited). *J. Appl. Phys.* **83,** 6385–6389 (1998).
24. Seshadri, R. *et al.* Study of the layered magnetoresistive perovskite $La_{1.2}Sr_{1.8}Mn_2O_7$ by high-resolution electron microscopy and synchrotron x-ray powder diffraction. *Chem. Mater.* **9,** 1778–1787 (1997).
25. Sloan, J., Battle, P. D., Green, M. A., Rosseinsky, M. J. & Vente, J. F. A HRTEM study of the Ruddlesden–Popper compositions $Sr_2LnMn_2O_7$ ($Ln =$ Y, La, Nd, Eu, Ho). *J. Solid State Chem.* **138,** 135–140 (1998).
26. Chudnovskii, F. A. The minimum conductivity and electron localisation in the metallic phase of transition metal compounds in the vicinity of a metal-insulator transition. *J. Phys. C* **11,** L99–L102 (1978).
27. Mott, N. F. *Metal–Insulator Transitions* (Taylor and Francis, 1974).
28. Ishikawa, T., Tobe, K., Kimura, T., Katsufuji, T. & Tokura, Y. Optical study on the doping and temperature dependence of the anisotropic electronic structure in bilayered manganites, $La_{2-2x}Sr_{1+2x}Mn_2O_7$ ($0.3 \leq x \leq 0.5$). *Phys. Rev. B* **62,** 12354–12362 (2000).
29. Takahashi, K., Kida, N. & Tonouchi, M. Optical evidence of a pseudogap in the ferromagnetic metallic phase of the bilayered manganite. *J. Magn. Magn. Mater.* **272,** E669–E670 (2004).
30. Okimoto, Y., Katsufuji, T., Ishikawa, T., Arima, T. & Tokura, Y. Variation of electronic structure in $La_{1-x}Sr_xMnO_3$ ($0 \leq x \leq 0.3$) as investigated by optical conductivity spectra. *Phys. Rev. B* **55,** 4206–4214 (1997).
31. Kimura, T. *et al.* Interplane tunneling magnetoresistance in a layered manganite crystal. *Science* **274,** 1698–1701 (1996).
32. Li, Q. A. *et al.* Reentrant orbital order and the true ground state of $LaSr_2Mn_2O_7$. *Phys. Rev. Lett.* **98,** 167201 (2007).
33. Zheng, H., Li, Q., Gray, K. E. & Mitchell, J. F. Charge and orbital ordered phases of $La_{2-2x}Sr_{1+2x}Mn_2O_{7-\delta}$. *Phys. Rev. B* **78,** 155103 (2008).
34. Sun, Z. *et al.* Electronic structure of the metallic ground state of $La_{2-2x}Sr_{1+2x}Mn_2O_7$ for $x = 0.59$ and comparison with $x = 0.36$, 0.38 compounds as revealed by ARPES. *Phys. Rev. B* **78,** 075101 (2008).
35. Chuang, Y-D., Gromko, A. D., Dessau, D. S., Kimura, T. & Tokura, Y. Fermi surface nesting and nanoscale fluctuating charge/orbital ordering in colossal magnetoresistive oxides. *Science* **25,** 1509–1513 (2001).
36. Kubota, M., Onoa, K. & Yoshida, T. Electronic structure of layered manganite $La_{1.1}Sr_{1.9}Mn_2O_7$ studied by angle-resolved photoemission spectroscopy at low temperatures. *J. Electron Spectrosc. Relat. Phenom.* **156-158,** 398–400 (2007).
37. Freeland, J. W. *et al.* Suppressed magnetization at the surfaces and interfaces of ferromagnetic metallic manganites. *J. Phys. Condens. Matter* **19,** 315210 (2007).
38. Freeland, J. W. *et al.* Full bulk spin polarization and intrinsic tunnel barriers at the surface of layered manganites. *Nature Mater.* **4,** 62–67 (2005).
39. Nascimento, V. B. *et al.* Surface-stabilized nonferromagnetic ordering of a layered ferromagnetic manganite. *Phys. Rev. Lett.* **103,** 227201 (2009).
40. de Jong, S. *et al.* High-resolution hard x-ray photoemission investigation of $La_{2-2x}Sr_{1+2x}Mn_2O_7$ ($0.30 < x < 0.50$): Microscopic phase separation and surface electronic structure of a bilayer colossal magnetoresistance manganite. *Phys. Rev. B* **80,** 205108 (2009).
41. van den Brink, J., Horsch, P. & Oleś, A. M. Photoemission spectra of $LaMnO_3$ controlled by orbital excitations. *Phys. Rev. Lett.* **85,** 5174–5177 (2000).
42. Bała, J., Sawatzky, G. A., Oleś, A. M. & Macridin, A. Quantum decoherence in the spectral function of undoped $LaMnO_3$. *Phys. Rev. Lett.* **87,** 067204 (2001).
43. Bała, J., Oleś, A. M. & Horsch, P. Quasiparticles and the structure of orbital polarons in ferromagnetic $LaMnO_3$. *Phys. Rev. B* **65,** 134420 (2002).
44. Daoud-Aladine, A., Rodríguez-Carvajal, J., Pinsard-Gaudart, L., Fernández-Díaz, M. T. & Revcolevschi, A. Zener polaron ordering in half-doped manganites. *Phys. Rev. Lett.* **89,** 097205 (2002).
45. Daoud-Aladine, A., Perca, C., Pinsard-Gaudart, L. & Rodríguez-Carvajal, J. Zener polaron ordering variants induced by A-site ordering in half-doped manganites. *Phys. Rev. Lett.* **101,** 166404 (2008).
46. Wohlfeld, K., Oleś, A. M. & Horsch, P. Orbitally induced string formation in the spin-orbital polarons. *Phys. Rev. B* **79,** 224433 (2009).
47. May, S. J. *et al.* Enhanced ordering temperatures in antiferromagnetic manganite superlattices. *Nature Mater.* **8,** 892–897 (2009).
48. Huang, X. Y., Mryasov, O. N., Novikov, D. L. & Freeman, A. J. Electronic and magnetic properties of layered colossal magnetoresistive oxides: $La_{1+2x}Sr_{2-2x}Mn_2O_7$. *Phys. Rev. B* **62,** 13318–13322 (2000).

Author contributions

F.M. and S.d.J. contributed equally to this work. M.S.G., J.B.G., S.d.J. and F.M. designed the experiments. Y.H., D.P. and A.T.B. grew the crystals. F.M., S.d.J., Y.H., W.K.S., I.S., A.M. and M.S.G. carried out the experiments. R.F., A.V., L.P. and M.S. provided photons and assistance during the synchrotron beamtimes. S.d.J and F.M. carried out the data analysis. S.d.J., F.M., J.B.G. and M.S.G. interpreted the results and wrote the paper, with feedback from co-authors.

Additional information

The authors declare no competing financial interests. Supplementary information accompanies this paper on www.nature.com/naturephysics. Reprints and permissions information is available online at http://www.nature.com/reprints. Correspondence and requests for materials should be addressed to M.S.G.